Two independent mouse lines carrying the Na(v)1.7 I228M gain-of-function variant display dorsal root ganglion neuron hyperexcitability but a minimal pain phenotype

Research Paper

PAIN®

Two independent mouse lines carrying the $Na_v1.7$ I228M gain-of-function variant display dorsal root ganglion neuron hyperexcitability but a minimal pain phenotype

Lubin Chen[a,b,c], Nivanthika K. Wimalasena[d,e], Jaehoon Shim[d,e], Chongyang Han[a,b,c], Seong-Il Lee[a,b,c], Rafael Gonzalez-Cano[d,e], Mark Estacion[a,b,c], Catharina G. Faber[f], Giuseppe Lauria[g,h], Sulayman D. Dib-Hajj[a,b,c], Clifford J. Woolf[d,e], Stephen G. Waxman[a,b,c,*]

Abstract

Small-fiber neuropathy (SFN), characterized by distal unmyelinated or thinly myelinated fiber loss, produces a combination of sensory dysfunction and neuropathic pain. Gain-of-function variants in the sodium channel $Na_v1.7$ that produce dorsal root ganglion (DRG) neuron hyperexcitability are present in 5% to 10% of patients with idiopathic painful SFN. We created 2 independent knock-in mouse lines carrying the $Na_v1.7$ I228M gain-of-function variant, found in idiopathic SFN. Whole-cell patch-clamp and multielectrode array recordings show that $Na_v1.7$ I228M knock-in DRG neurons are hyperexcitable compared with wild-type littermate-control neurons, but despite this, $Na_v1.7$ I228M mice do not display mechanical or thermal hyperalgesia or intraepidermal nerve fiber loss in vivo. Therefore, although these 2 $Na_v1.7$ I228M knock-in mouse lines recapitulate the DRG neuron hyperexcitability associated with gain-of-function mutations in $Na_v1.7$, they do not recapitulate the pain or neuropathy phenotypes seen in patients. We suggest that the relationship between hyperexcitability in sensory neurons and the pain experienced by these patients may be more complex than previously appreciated and highlights the challenges in modelling channelopathy pain disorders in mice.

Keywords: $Na_v1.7$, I228M, Small-fiber neuropathy, $Na_v1.7$ I228M knock-in mouse, Targeted homologous recombination, CRISPR, Hyperexcitability, IENF, Neuropathy, Pain

1. Introduction

The voltage-gated sodium channel $Na_v1.7$ is a key determinant of nociceptor excitability and a major contributor to pain signalling in humans. Gain-of-function mutations of *Scn9a*, the gene that encodes $Na_v1.7$, are associated with a spectrum of chronic pain conditions, including rare heritable syndromes such as inherited erythromelalgia and paroxysmal extreme pain disorder, as well as more common acquired pain disorders, such as painful diabetic neuropathy and small-fiber neuropathy (SFN).[1,6] Unlike diabetic polyneuropathy, which can involve all classes of fibers, SFN is characterized by damage to unmyelinated C fibers and thinly myelinated Aδ-afferent fibers, as indicated by quantitative sensory testing and the degeneration of intraepidermal nerve fibers (IENFs) in the skin.[3,4] Consistent with a selective involvement of small-diameter fibers, the clinical presentation of SFN is characterized by a combination of pain, sensory deficits, and autonomic complaints.[10] Small-fiber neuropathy can be associated with multiple diseases, such as diabetes mellitus or autoimmune disorders, but is idiopathic in a substantial proportion (approximately 50%) of patients.[15]

The mechanism underlying distal axon degeneration and pain symptoms in SFN is not well understood. However, the identification of gain-of-function $Na_v1.7$ variants in idiopathic SFN cases provides an avenue for investigating possible underlying molecular mechanisms.[9] Small-fiber neuropathy-associated $Na_v1.7$ variants render dorsal root ganglion (DRG) neurons hyperexcitable, as demonstrated by abnormal spontaneous firing, lower action potential firing threshold, and enhanced firing frequency.[9] Importantly, these mutations produce changes in the gating properties of $Na_v1.7$ channels, such as impaired slow inactivation, depolarized slow and/or fast inactivation, or enhanced resurgent current.[9] Among the SFN $Na_v1.7$ mutations, I228M is of particular interest because patients carrying this mutation experience a relatively early clinical onset (within first 3 decades).[8,9] A major unanswered question is whether the pain in these patients is secondary to

Sponsorships or competing interests that may be relevant to content are disclosed at the end of this article.

L. Chen and N.K. Wimalasena contributed equally to this work.

C.J. Woolf and S.G. Waxman contributed equally to this work.

[a] Department of Neurology, Yale University School of Medicine, New Haven, CT, United States, [b] Center for Neuroscience and Regeneration Research, Yale University School of Medicine, New Haven, CT, United States, [c] Center for Rehabilitation Research, VA Connecticut Healthcare System, West Haven, CT, United States, [d] FM Kirby Neurobiology Center, Boston Children's Hospital, Boston, MA, United States, [e] Department of Neurobiology, Harvard Medical School, Boston, MA, United States, [f] Department of Neurology, School of Mental Health and Neuroscience, Maastricht University Medical Center, Maastricht, the Netherlands, [g] Neuroalgology Unit, IRCCS Foundation, "Carlo Besta" Neurological Institute, Milan, Italy, [h] Department of Biomedical and Clinical Sciences, "Luigi Sacco", University of Milan, Milan, Italy

**Corresponding author. Address: Neuroscience and Regeneration Research Center, VA Connecticut Healthcare System, 950 Campbell Ave, Bldg 34, West Haven, CT 06516, United States. Tel.: (203) 937-3802; fax: (203) 937-3801. E-mail address: stephen.waxman@yale.edu (S.G. Waxman).*

PAIN 162 (2021) 1758–1770

http://dx.doi.org/10.1097/j.pain.0000000000002171

the neuropathy or the consequence of nociceptor hyperexcitability. Dorsal root ganglion neurons transfected with human $Na_v1.7$ I228M channels exhibit a significant (~20%) reduction in neurite length[14] suggesting that the hyperexcitability may be linked to the neuropathy. Mechanistic investigations have demonstrated that reverse operation (Ca^{2+} importing) of the Na^+/Ca^{2+} exchanger (NCX)[14] and damaged mitochondrial energy metabolism[12] may contribute to the impaired neurite integrity present in $Na_v1.7$ I228M-transfected DRG neurons.

Although in vitro studies have provided valuable insights into the underlying pathophysiology of the symptoms seen in patients with SFN, models using overexpression of a mutant $Na_v1.7$ 1228M channel do not recapitulate the situation in patients. In this study, we report the phenotypes of 2 $Na_v1.7$ I228M knock-in ($Na_v1.7^{I228M}$) mouse lines generated independently in separate laboratories, by targeted homologous recombination or CRISPR editing. We investigate the physiological properties of their DRG neurons, assess morphological changes in axons and IENFs, and search for behavioural correlates of the pain symptoms found in patients.

2. Methods

2.1. Generation of $Na_v1.7^{I228M}$ knock-in mice

2.2.1. $Na_v1.7^{I228M}$ knock-in mouse line by targeted homologous recombination

Scn9a p.I228M knock-in mice were generated by inGenious Targeting Laboratory (Ronkonkoma, NY) using a targeted homologous recombination approach. Briefly, targeted iTL BF1 (C57BL/6 FLP) embryonic stem cells carrying the targeted I228M Scn9A mutant allele and the neomycin selection cassette were microinjected into Balb/c blastocysts. Resulting chimeras with a high-percentage black coat color were mated with C57BL/6 WT mice to generate germline Neo deleted mice. Final germline-transmitted mice were confirmed for the deletion of the Neomycin cassette and the presence of the p.I228M allele by genotyping tail DNA from mice with black coat color, and sequencing the PCR product. A founder line was backcrossed to wild-type C57BL/6J for 6 generations before it was used for behavioural and electrophysiological assays.

2.2.2. $Na_v1.7^{I228M}$ knock-in mouse line by CRISPR editing

Fertilized embryos from pregnant female C57BL/6J mice were used to generate mice with the I228M mutation in *Scn9a* ($Na_v1.7$). Fertilized embryos were removed and injected with Cas9 mRNA, synthetic CRISPR guide RNAs, and a ssDNA donor sequence containing the base pair change to effect the desired mutation as well as 5 silent mutations. They were then placed into a donor mother and carried to term.

gRNA sequences: ATTCCAGGTAAGAAGTGATTGG and CACACCAATCACTTCTTACCTGGI. 228M ssDNA donor sequence (103 bp): CAG CTC TTC GAA CTT TCA GAG TCT TGA GAG CTT TGA AAA CTA TTT CCG TTA TGC CGG GAA AGA AGT GAT TGG TGT GGA GCT TTA GAC TGC TCA ACT CCA GCT G.

The resulting offspring were genotyped by PCR and Sanger sequencing. It was confirmed that 2 mice had an insertion of the desired ssDNA; one heterozygote and one homozygote founder. These mice were then each bred with wild-type mice to generate a colony.

PCR primers. Forward: ACC TAG GCA ATG TTT CAG CTC TTC G.

Reverse**: CTT CCT TCT CCA AGA CCC ATG CAA.

**used for sequencing.

2.3. Patch-clamp recordings

Dorsal root ganglion neurons from 4 to 8 weeks $Na_v1.7$ WT or $Na_v1.7^{I228M}$ knock-in mice by targeted homologous recombination (both sexes) were cultured using a protocol as previously described.[5] Whole-cell current-clamp recordings were obtained from small-diameter (<25 μm) DRG within 24 hours after culture by using an EPC-9 amplifier and Pulse 8.5 (HEKA, Germany). Electrodes (1-3 MΩ) were filled with pipette solution (mM): 140 KCl, 0.5 EGTA, 5 HEPES, 3 Mg-ATP, and pH 7.3 with KOH (adjusted to 315 mOsm with dextrose). The extracellular solution contained (mM): 140 NaCl, 3 KCl, 2 $MgCl_2$, 2 $CaCl_2$, 10 HEPES, and pH 7.3 with NaOH (adjusted to 320 mOsm with dextrose). Whole-cell configuration was obtained in a voltage-clamp mode before proceeding to current clamp. Cells with stable resting membrane potentials were used for data collection by PatchMaster (HEKA-Electronics) software.

Electrophysiological data were analyzed using Fitmaster (HEKA-Electronics) and Origin 8.5 (Microcal, Northampton, MA) and SPSS Statistics 24 (IBM) and were presented as means ± SE. For multigroup statistical analysis, we used one-way ANOVA followed by the Tukey *post hoc* test or Kruskal–Wallis test followed by the Dunn procedure depending on whether data showed a normal distribution. The 2-proportions *z* test was used to compare the proportion of spontaneously firing neurons.

2.4. Multielectrode array

Dissociated DRG neurons from 6 to 9-week-old WT (n = 3, 2 females and 1 male) and $HomNa_v1.7^{I228M}$ knock-in mice by targeted homologous recombination (n = 4, 2 females and 2 males) were maintained at 37°C in a 5% CO_2 incubator for 3 days before multielectrode array (MEA) recordings. Action potential firing was measured using a multiwell-MEA system (Maestro; Axion Biosystems, Atlanta, GA). A 12-well recording plate with 768 electrodes was used. For each experiment, neurons from WT or $HomNa_v1.7^{I228M}$ mice were dissociated and plated at the same time in 6 wells each. The investigator was blinded to the identity of neurons. Precise temperature control of the MEA system was used to create temperature ramps and maintain temperatures at 30°, 33°, 37°, 40°, and 43°C each for 200 seconds. The size of the observed signal is impacted by many factors that include the current density of the neuron as well as the geometry (distance) between the neuron and the electrode. We apply strict criteria for neuron plating to ensure comparable cell density per well, and data analysis with the signal to noise of spike detection is achieved by setting the threshold for a spike detection criterion of >6 standard deviation (SD) above background signals. Electrodes registering >5 recorded spikes over 200 seconds period were determined as active. The number of active electrodes and mean firing frequency were measured. Data were analysed using Axion Integrated Studio AxIS 2.1 (Axion Biosystems) and NeuroExplorer (NexTechnologies, Madison, AL). Statistical significance was determined using the Mann–Whitney *U* test. Data are expressed as mean ± SEM. A P value of < 0.05 was considered significant.

2.5. Behavioural assays

2.5.1. $Na_v1.7$ I228M knock-in mouse line by targeted homologous recombination

All animal procedures were conducted in accordance with the NIH's Guide for the Care and Use of Laboratory Animals and were

approved by the IACUC of the Veterans Administration Connecticut Health care System. Adult mice (8-12 weeks old) of both sexes were used in this study.

2.5.1.1. Hot plate

Animals were placed on a metal plate (Hot Plate Analgesia Test Meter; IITC, Woodland Hills, CA) uniformly heated to a constant temperature of 52°C. The response latency for first licking or flinching of the hind paws was recorded. The mice were immediately removed from the hot plate on showing nocifensive behaviors or if no response occurred within the 30 seconds cutoff time.

2.5.1.2. Hargreaves test

Animals were placed on a glass plate, and plantar paw surface was exposed to radiant heat using a Hargreaves apparatus (IITC), and the paw withdrawal latency was measured. The heat stimulation was repeated 3 times on both paws, with at least 5 minutes rest between consecutive tests. The cutoff value was set at 30 seconds to prevent tissue damage.

2.5.1.3. von Frey test

Animals were placed on an elevated wire grid, and the plantar surface of both paws was presented with a series of calibrated von Frey filaments (Stoelting, Wood Dale, IL). Each filament was applied for 5 seconds. A nocifensive response was recorded when flinching, withdrawal, paw licking, or toe spreading was observed. The 50% withdrawal threshold was determined using the "up–down" method that requires 6 stimuli straddling the threshold. At least 5 minutes of rest were allowed between each stimulus.

2.5.1.4. Thermal gradient test and preference test

The thermal preference apparatus consisted of 2 heating/cooling plates (Bioseb, Chaville, France) placed side by side and enclosed in a plexiglass chamber. The temperatures of test and reference plates were set to 35 vs 25°C, 15 vs 25°C, or 38 vs 33°C. Animal movements were recorded for 600 seconds by an automated infrared camera tracking system. The time spent on the reference and test plates was calculated. The thermal gradient apparatus maintained a stable temperature gradient from about 6°C to 46°C using the 2 heating/cooling devices positioned at each end of a metal floor. The floor area was divided into 10 zones, each with a stable temperature measured using a thermometer (TM-3 three-scale temperature monitor, Warner Instruments, Hamden, CT). Tracking was performed using software provided by the manufacturer, and the time spent in each zone over the 60-minute test period was determined.

2.5.1.5. Formalin test

Mice were habituated to observation chambers for at least 30 minutes before experiments. For induction of short-term inflammation, 10 μL of 5% formalin was injected subcutaneously (s.c.) into the plantar surface of the left hind paw. After injection, mice were immediately returned to the observation chamber and nociceptive behaviours (licking, flicking, and lifting the injected paw) were recorded for 45 minutes. The duration of formalin-induced nociceptive behaviors in 5-minute intervals was scored by an experimenter blind to treatment or genotype.

2.5.1.6. Complete Freund's adjuvant injections

Mice were anaesthetized by exposure to isoflurane (1%-3%) administered by a calibrated vaporizer. For induction of long-term inflammation, 10 μL of complete Freund's adjuvant (CFA; Sigma, containing 1 mg/mL of *Mycobacterium tuberculosis*) was injected into the left hind paw using a 10 μL-Hamilton syringe (Hamilton company, Reno, Nevada).

2.5.2. $Na_v1.7$ I228M knock-in mouse line by CRISPR editing

All mouse study at the Boston Children Hospital was performed in accordance with the IACUC protocol 17-06-3494R. Eight to 12-week-old mice of both sexes were used in these studies.

2.5.2.1. von Frey

These experiments were performed following the standard protocol. Briefly, animals (n = 7 for WT, n = 5 for $HetNa_v1.7^{I228M}$, and n = 8 for $HomNa_v1.7^{I228M}$) were placed on an elevated wire grid in a plastic enclosure and habituated twice for 2 hours preceding the day of measurement. On the testing day, they were habituated for 1 hour before probing the right hind paw with von Frey filaments. All animals were tested with the 0.6 g filament first, and then we proceeded using the up–down method.

2.5.2.2. Hot plate

The hot plate was set at 50°C. Animals (n = 9 for WT, n = 9 for $HetNa_v1.7^{I228M}$, and n = 5 for $HomNa_v1.7^{I228M}$) were placed on the plate, and the latency to licking the hind paw or jumping was recorded. After 60 seconds, the mice were removed from the plate if there was no response. Mice were tested only once to ensure they did not adapt to the assay.

2.5.2.3. Thermal gradient

The thermal gradient assay was evaluated as previously described (PMID: 28481358). A continuous temperature gradient (5-50°C) was established along a metallic base plate (Bioseb, France) on which the mice (n = 7 for WT, n = 10 for $HetNa_v1.7^{I228M}$, and n = 4 for $HomNa_v1.7^{I228M}$) walked freely while video was recorded from above (Noldus, VA). Each evaluation lasted 1.5 hours, and 2 mice were recorded simultaneously in separate corridors. Each corridor was virtually divided into 20 zones of equal size (6 cm) with a different and stable temperature. After a period of exploration (60 minutes), the mouse showed a clear preference, indicating the most comfortable temperature range.

2.5.3. Immunohistochemistry for intraepidermal nerve fiber density in the skin

Eight to 12-week-old WT and $Nav1.7^{I228M}$ knock-in mice by targeted homologous recombination (n = 4 each genotype; both sexes) were anesthetized with ketamine/xylazine (100/10 mg/kg, i.p.) and transcardially perfused with 0.01M PBS (pH 7.4) followed by ice-cold 4% paraformaldehyde in 0.14 M Sorensen's phosphate buffer (pH 7.4). Same regions of ventral hind paw glabrous skin were removed using 3-mm biopsy punch. Foot pad skin tissues were removed, immersion-fixed in 4% paraformaldehyde (total fixation time 20 minutes) and cryoprotected with 30% (wt/vol) sucrose in PBS overnight at 4°C. Tissue sections were cut on a cryostat at 10 μm and mounted on slides (Fisher Scientific, Pittsburgh, PA). Sections were immediately processed for the detection of target protein or stored at −20°C for future use.

Sections were incubated in the following solutions: (1) blocking solution (PBS containing 4% normal donkey serum, 2% BSA, 0.1% Triton X-100, and 0.02% sodium azide) for 1 hour at room temperature; (2) rabbit monoclonal anti-PGP 9.5 antibody (1:300, Abcam, Cat# ab108986, Batch# GR3231441-1) in blocking solution at 4°C overnight; (3) PBS, 3 × 10 minutes each; (4) Alexa Fluor 546-conjugated donkey

anti-rabbit IgG (H + L) secondary antibody (1:1000; Invitrogen, Carlsbad, CA) in blocking solution for 1 hour at room temperature; and (5) PBS, 3 × 10 minutes. Tissue sections were mounted in antifade mounting medium with DAPI (H-1500, Vectashield) and were examined with a Nikon Eclipse E800 fluorescence microscope or a Nikon C1 confocal microscope (Nikon USA, Melville, NY).

2.6. Light microscopy analysis of axons in the sciatic nerve

Eight to 12-week-old WT or $Na_v1.7^{I228M}$ knock-in mice by targeted homologous recombination (both sexes) were anesthetized with ketamine/xylazine (100/10 mg/kg, i.p.) and transcardially perfused with 0.01M PBS (pH 7.4), followed by ice-cold 4% paraformaldehyde in 0.14 M Sorensen's phosphate buffer (pH 7.4). The sciatic nerves at the midthigh level (distal to the trifurcation) were dissected and transferred to 2% paraformaldehyde plus 2% glutaraldehyde in 0.14 M Sorensen's phosphate buffer (pH 7.4) at 4°C overnight. Samples were then postfixed with 1% osmium (Polysciences, Warrington, PA), dehydrated and blocked in 0.5-cm segments, and embedded in Epox-812 (Ernest F. Fullam, Latham, NY) using standard plastic embedding protocols. Semithin sections (1 μm) were collected from each tissue block and counterstained with methylene blue and azure II (0.5% each in 0.5% borax) for light microscopy. Sections were examined with a Nikon Ti Eclipse microscope, and digital images were recorded with Nikon NIS-Elements imaging software.

2.7. Neurite growth assay

2.7.1. $Na_v1.7$ I228M knock-in mouse line by targeted homologous recombination

Dorsal root ganglion neurons were isolated from 6 to 8-week-old WT and $Na_v1.7$ I228M mice (both sexes) and electroporated with the plasmid encoding red fluorescent protein. After the electroporation, cells were plated on the coverslips coated with laminin and cultured for 7 days. The resulting cultures were imaged and their total lengths per cell were assessed. Each experiment includes cultures from a pair of age/sex-matched WT and $Na_v1.7$ I228M mutant mice. Dorsal root ganglion neurons from each mouse are plated onto 3 to 4 culture dishes. Each data point represents the total neurite length per cell within one culture dish. Data are normalized to the average WT values of the same experiment and presented as mean ± SD.

2.7.2. $Na_v1.7$ I228M knock-in mouse line by CRISPR editing

2.7.2.1. Dorsal root ganglion culture

Dorsal root ganglia were dissected from 8 to 12-week-old mice, and then dissociated and cultured according to the standard protocol. Briefly, the samples were digested with Collagenase/Dispase and mechanically triturated in the presence of DNAse until a single-cell suspension was formed. Debris was removed using a BSA gradient. The neurons were then plated at a density of 1000 cells/well in a 96-well plate coated with PDL/laminin. Cells were grown in a Neurobasal medium supplemented with PenStrep, B27, L-glutamine, NGF, GDNF, and AraC.

2.7.2.2. Neurite outgrowth

After 24 hours, the cells were fixed using 4% PFA and stained with Tuj1 and DAPI. The plates were then imaged on the ArrayScan system (*Thermo Fischer*) at ×10 magnification. Cell bodies and neurites were automatically detected by the system and used to quantify neurite length per neuron within each well.

2.7.2.3. Spot culture

Instead of plating in a 96-well plate, 30k DRG neurons were plated in a single spot (7 uL volume) in the center of a 35-mm dish coated with PDL/laminin. After the cells had time to adhere (30 minutes), the rest of the media volume was added to the dish, with special care taken not to disturb the spot. The spots were then grown for up to 6 days and imaged on alternate days using brightfield microscopy. On the sixth day, the spots were fixed with 4% PFA and stained with Tuj1. They were imaged at ×10 magnification using an 8 × 8 tile, such that the 64 images captured the entirety of each spot.

2.7.2.4. Sholl analysis

Sholl analysis was used to quantify neurite length. Briefly, the background of the image was removed, and then the image was thresholded such that neurites were easily visible. Then, using a macro in ImageJ, concentric circles were created around the center spot, and intersections of neurites with these circles were quantified. The diameter of each ring was then plotted against the number of intersections and a proxy for the number of neurites of a given length.

3. Results

3.1. Small-diameter dorsal root ganglion neurons from $Na_v1.7^{I228M}$ mutant mice are hyperexcitable

Knock-in mice, of both sexes, produced by targeted recombination were used for these studies. Using current-clamp recordings, we compared the excitability of small-diameter (<25 μm) DRG neurons from heterozygous (Het) and homozygous (Hom) $Na_v1.7^{I228M}$ mutant mice with their wild-type (WT) littermate controls. A series of 200-millisecond depolarizing currents in 5 pA increments were used to determine the current threshold for the first all-or-none action potential. **Figure 1A** shows representative action potential traces from a small-diameter WT DRG neuron in response to graded membrane potential depolarizations, where an overshooting action potential was produced at a threshold of 125 pA. By contrast, representative action potentials recorded from $HetNa_v1.7^{I228M}$ (**Fig. 1B**) and $HomNa_v1.7^{I228M}$ (**Fig. 1C**) DRG neurons showed current thresholds of 60 pA and 55 pA, respectively. The average current threshold was significantly reduced (by half) in small-diameter DRG neurons from $HetNa_v1.7^{I228M}$ mice (62 ± 9 pA, n = 23, $P < 0.05$) and $HomNa_v1.7^{I228M}$ mice (56 ± 10 pA, n = 23, $P < 0.01$) compared with DRG neurons from WT mice (118 ± 19 pA, n = 28) (**Fig. 1D**). Resting membrane potential (RMP) was also significantly depolarized in neurons from $HetNa_v1.7^{I228M}$ (−53.2 ± 1.2 mV, n = 23; $P < 0.05$) and $HomNa_v1.7^{I228M}$ (−52.9 ± 1.1 mV, n = 23; $P < 0.05$) mutant mice, compared with neurons from WT groups (−57.4 ± 1.1 mV, n = 28) (**Fig. 1E**). There was no statistically significant difference in input resistance (WT: 1.0 ± 0.1 GΩ, n = 28; $HetNa_v1.7^{I228M}$: 1.2 ± 0.1 GΩ, n = 23; $HomNa_v1.7^{I228M}$: 1.3 ± 0.1 GΩ, n = 23), action potential amplitude (WT: 120.1 ± 1.7 mV, n = 28; $HetNa_v1.7^{I228M}$: 117.2 ± 1.6 mV, n = 23; $HomNa_v1.7^{I228M}$: 117.7 ± 1.6 mV, n = 23), or action potential half-width (WT: 4.27 ± 0.18 ms, n = 28; $HetNa_v1.7^{I228M}$: 4.37 ± 0.23 ms, n = 23; $HomNa_v1.7^{I228M}$: 4.43 ± 0.17 mV, n = 23) among the 3 groups.

We next investigated the responses of small-diameter DRG neurons from WT, $HetNa_v1.7^{I228M}$, and $HomNa_v1.7^{I228M}$ mice to a series of 500-millisecond sustained depolarizations. Representative action potential firing traces demonstrated that, compared with WT controls, small-diameter DRG neurons from $HetNa_v1.7^{I228M}$ and $HomNa_v1.7^{I228M}$ mice generated more action potentials in response to 3x

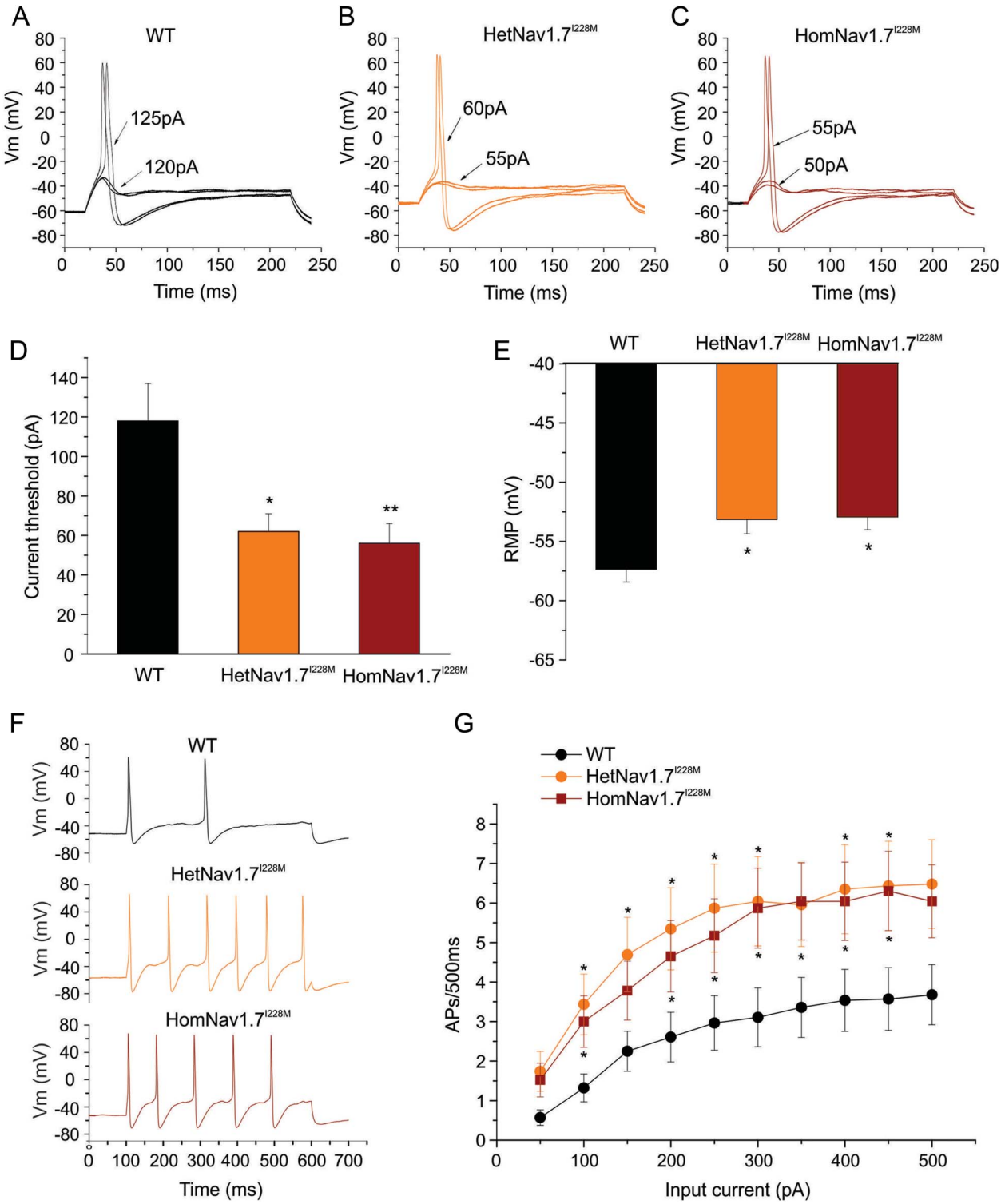

Figure 1. Small-diameter DRG neurons from HetNa$_v$1.7^{I228M} and HomNa$_v$1.7^{I228M} mutant mice are hyperexcitable compared with WT control DRG neurons. (A) Representative traces of a small-diameter DRG neuron from a WT mouse, showing subthreshold responses to current injections up to 120 pA and subsequent action potentials evoked by current injections above 125 pA (the current threshold for this neuron). (B) Representative traces of a small-diameter DRG neuron from a HetNa$_v$1.7^{I228M} mouse, showing a lower current threshold (60 pA) for action potential generation. (C) Representative traces of a small-diameter DRG neuron from a HomNa$_v$1.7^{I228M} mouse, showing a lower current threshold (55 pA) for action potential generation. (D) Small-diameter DRG neurons from HetNa$_v$1.7^{I228M} and HomNa$_v$1.7^{I228M} mice display significantly reduced current threshold compared with WT control neurons (*$P < 0.05$; **$P < 0.01$, one-way ANOVA, followed by the Tukey *post hoc* test). (E) Small-diameter DRG neurons from HetNav1.7^{I228M} and HomNav1.7^{I228M} mice display significantly depolarized RMP compared with WT-control neurons (* $P < 0.05$, one-way ANOVA, followed by the Tukey *post hoc* test). (F) Representative responses of small-diameter DRG neurons from WT, HetNa$_v$1.7^{I228M}, and HomNa$_v$1.7^{I228M} mice, respectively, to 500 milliseconds depolarizing current 3× the threshold for action potential generation. (G) Comparison of firing frequency of small-diameter DRG neurons from WT, HetNa$_v$1.7^{I228M}, and HomNa$_v$1.7^{I228M} mutant mice, in response to graded 500 milliseconds depolarising current stimuli from 50 to 500 pA in 50 pA increments. Na$_v$1.7^{I228M} mutant groups show significantly higher firing frequencies compared with the WT group (* $P < 0.05$, one-way ANOVA, followed by the Tukey *post hoc* test). ANOVA, analysis of variance; DRG, dorsal root ganglion; RMP, resting membrane potential; WT, wild type.

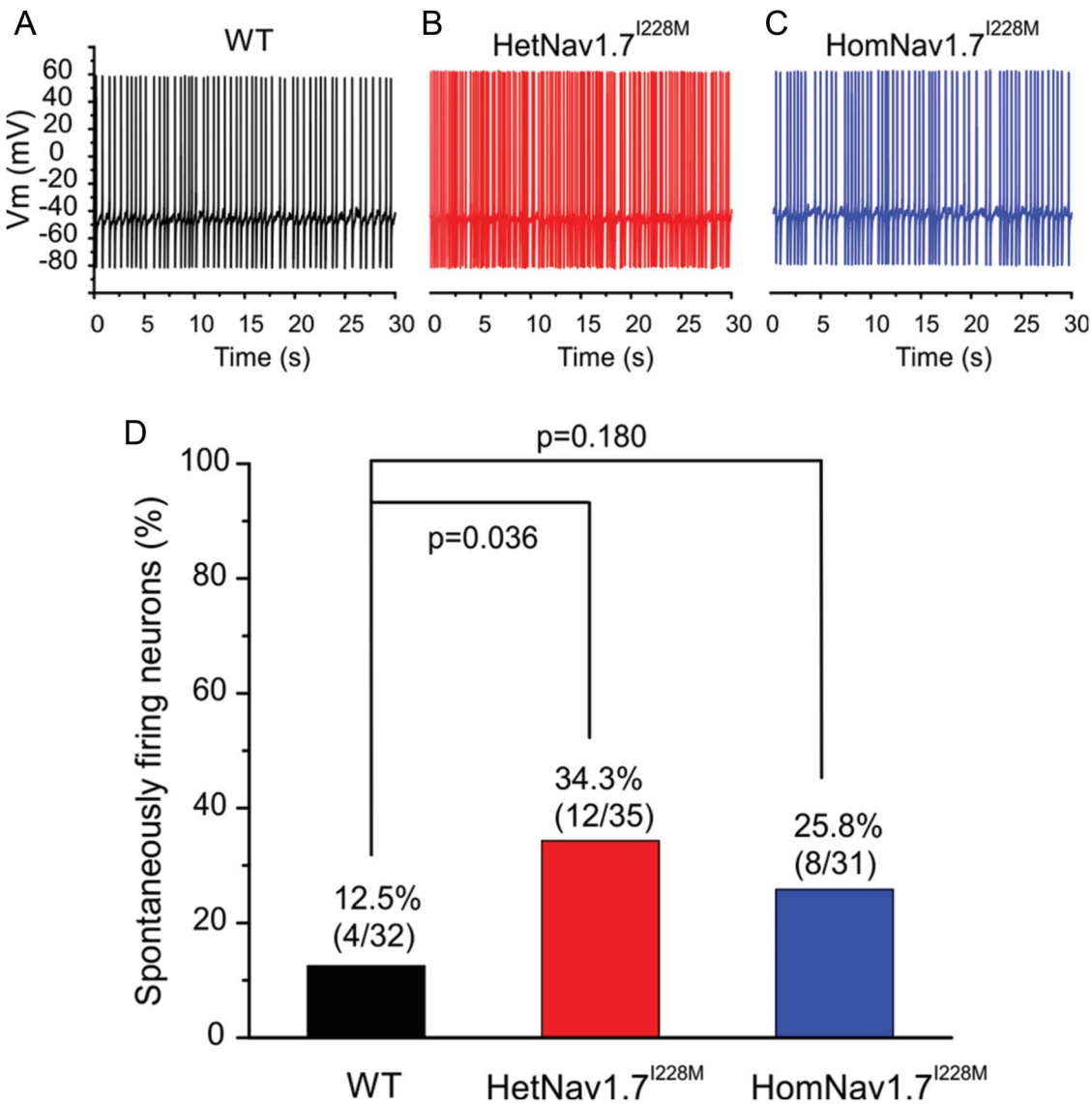

Figure 2. Spontaneously active DRG neurons. Representative recordings showing spontaneous firing (30 seconds) of DRG neurons from WT (A), HetNa$_v$1.7^{I228M} (B), and HomNa$_v$1.7^{I228M} (C) mice. Trace was recorded for 30 seconds without current injection. (D) Comparison of the proportion of spontaneously firing DRG neurons among WT, HetNa$_v$1.7^{I228M}, and HomNa$_v$1.7^{I228M} groups. Compared with WT group, HetNa$_v$1.7^{I228M}, and HomNa$_v$1.7^{I228M} groups displayed an increased proportion of spontaneously firing neurons but reached statistical significance only for the HetNav1.7^{I228M} group (the 2-proportions *z* test was used to compare the proportion of spontaneously firing neurons). DRG, dorsal root ganglion; WT, wild type.

threshold current injections (**Fig. 1F**). As summarized in **Figure 1G**, compared with WT controls, small-diameter DRG neurons from HetNa$_v$1.7^{I228M} and HomNa$_v$1.7^{I228M} mice generated significantly more action potential firing in response to the current injections.

There was also an increased proportion of spontaneously firing neurons in both HetNa$_v$1.7^{I228M} and HomNa$_v$1.7^{I228M} mice (**Fig. 2**). 34.3% (12 of the 35 neurons, $P < 0.05$) HetNa$_v$1.7^{I228M} DRG neurons and 25.8% (8 of the 31 neurons) HomNa$_v$1.7^{I228M} DRG neurons were spontaneously active, whereas only 4 of the 32 (12.5%) recorded DRG neurons from WT mice displayed spontaneous firing.

3.2. Dorsal root ganglion neurons from Na$_v$1.7^{I228M} mutant mice show enhanced responses to noxious heat in vitro

We recorded action potential firing of cultured DRG neurons from WT and HomNav1.7^{I228M} mice (produced by targeted recombination) by an MEA, an extracellular recording approach that permits the study of the firing of many neurons without rupturing the membrane and dialyzing their content as in the current-clamp recordings. We examined activity at baseline temperature (30˚C), skin temperature (33˚C), core body temperature (37˚C), nonnoxious warmth (40˚C), and noxious heat (43˚C). Representative raw traces of a 10-second epoch (**Fig. 3A**) show that DRG neurons from WT and HomNa$_v$1.7^{I228M} mutant mice both produced clearly identifiable spikes, which exhibited a reproducible waveform in the MEA recordings in the absence of stimulation. Representative heat-map plots of active electrode (colored circles) and fired action potentials (color scale) showed a difference in response to increasing temperatures between DRG neurons from WT and HomNa$_v$1.7^{I228M} mutant mice (**Fig. 3B**). Compared with WT controls, the HomNa$_v$1.7^{I228M} group had significantly more active electrodes (WT: 1.9 ± 0.4; HomNa$_v$1.7^{I228M}: 3.5 ± 0.7 active electrodes per well; $P < 0.05$) at the noxious temperature 43˚C (**Fig. 3B**), although the mean action potential firing frequency in those active electrodes seemed to be similar (**Fig. 3C**). In addition, we observed that neurons from

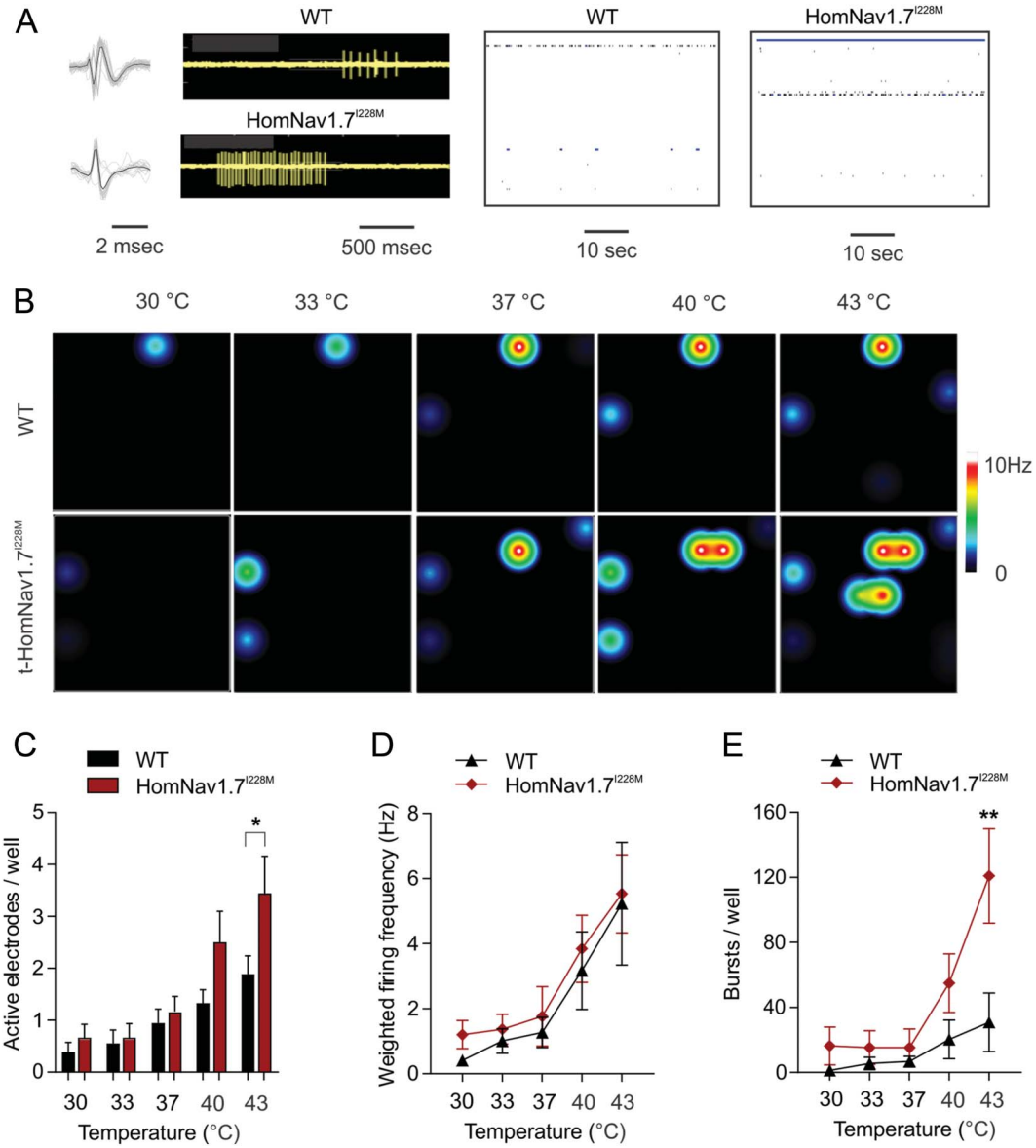

Figure 3. DRG neurons from HomNav1.7^{I228M} mutant mice show an enhanced response to heat in MEA recordings. (A) Representative spike waveforms (left panels) recorded using an MEA from DRG neurons expressing WT and HomNa$_v$1.7^{I228M} mutant mice. Black line indicates the averaged waveform from 20 individual spikes. Grey lines indicate individual spikes. Raw traces from a single-electrode recording DRG neurons from WT and HomNa$_v$1.7^{I228M} mutant mice (middle panels). DRG neurons from HomNav1.7^{I228M} mutant mice produce more bursts compared with those from WT mice in the same recording period. A well-wide (64 electrodes) raster plot of MEA recordings of DRG neurons from WT and HomNa$_v$1.7^{I228M} at 40°C. Each horizontal plot represents recording from one electrode. More electrodes recorded spikes from DRG neurons from HomNav1.7^{I228M} than WT mice. The blue plots indicate burst firing as defined by default setting of the Axion analysis software. (B) Representative heat-map plots of MEA recordings of DRG neurons from WT and HomNav1.7^{I228M} mutant mice at 30, 33, 37, 40, and 43°C. Each colored circle represents an active electrode within an 8 × 8 electrode array. More active electrodes and higher firing frequency are recorded at higher temperatures. More active electrodes are seen in wells containing HomNa$_v$1.7^{I228M} mutant DRG neurons. (C) The number of active electrodes in WT and HomNa$_v$1.7^{I228M} groups at temperatures 30, 33, 37, 40, and 43°C. The HomNa$_v$1.7^{I228M} group displays significantly more active electrodes compared with the WT group at 43°C (* $P < 0.05$, Mann–Whitney *U* test). (D) Weighted firing frequencies of DRG neurons from WT and HomNa$_v$1.7^{I228M} mutant mice. No significant difference is seen between groups. (E) The number of bursts in DRG neurons from WT and HomNa$_v$1.7^{I228M} mutant mice. The HomNa$_v$1.7^{I228M} group displays significantly more bursts compared with the WT group at 43°C (** $P < 0.01$, Mann–Whitney *U* test). DRG, dorsal root ganglion; MEA, multielectrode array; WT, wild type.

HomNa$_v$1.7^{I228M} mice fired significantly more bursts (>5 spikes) than WT neurons (WT: 30.9 ± 18.0; HomNa$_v$1.7^{I228M}: 120.9 ± 29.0 bursts per well; $P < 0.01$) (**Fig. 3D**).

3.3. Basal and inflammatory pain behaviors are normal in Na$_v$1.7^{I228M} mutant mice

Given the robust hyperexcitability of cultured DRG neurons from Na$_v$1.7 ^{I228M} mice and their enhanced response to noxious heat, we anticipated that pain behaviour in the mutant mice might be augmented and recapitulate aspects of the human clinical phenotype. However, surprisingly Na$_v$1.7^{I228M} mutant mice produced by targeted homologous recombination did not display any significant changes in thermal or mechanical pain thresholds compared with littermate controls. Although HetNa$_v$1.7^{I228M} and HomNa$_v$1.7^{I228M} mutant mice showed a trend toward a reduction in the thermal pain threshold in the hot-plate (52°C) test, this did not reach statistical significance overall, nor in female or male subgroups (**Fig. 4A**). Withdrawal thresholds to thermal

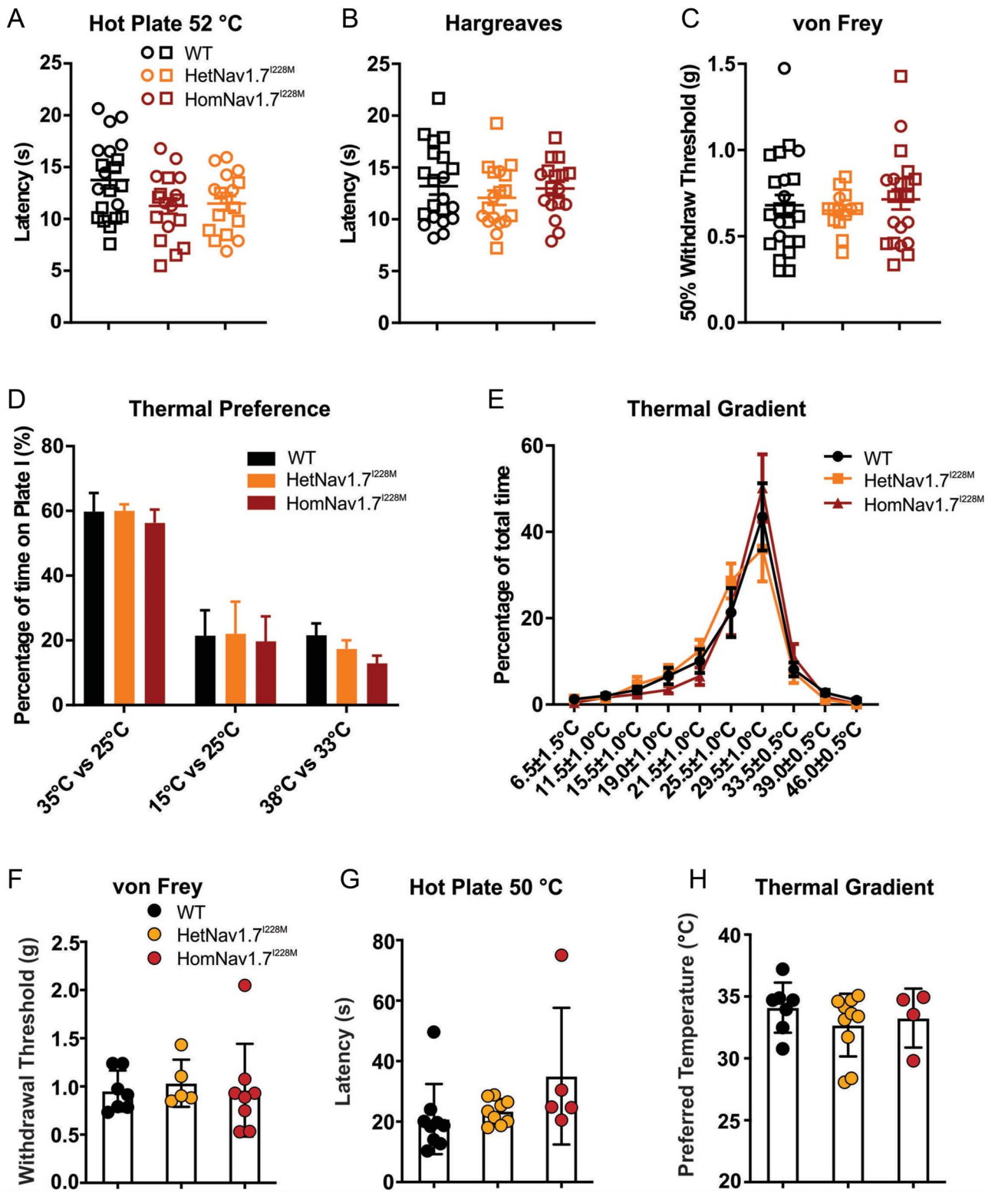

Figure 4. $Na_v1.7^{I228M}$ mutant mice do not show thermal or mechanical hypersensitivity. (A) The hot-plate test at 52°C. There is a trend toward lower thermal thresholds in $Na_v1.7^{I228M}$ mutant mice ($HetNa_v1.7^{I228M}$, n = 18; $HomNa_v1.7^{I228M}$, n = 17), but the difference compared with wild type (WT)-control littermates (n = 21) does not reach statistical significance. Open circle and square represent female and male mice, respectively. (B) Thermal thresholds measured by the Hargreaves test. No significant difference between WT (n = 21), $HetNa_v1.7^{I228M}$ (n = 18), and $HomNa_v1.7^{I228M}$ (n = 17) groups. (C) Mechanical thresholds measured by the von Frey test. No significant difference between WT (n = 23), $HetNa_v1.7^{I228M}$ (n = 14), and $HomNa_v1.7^{I228M}$ (n = 21) groups. (D) The thermal place preference test: the percentage of time spent at a test temperature vs control temperature (35 vs 25°C, 15 vs 25°C, and 38 vs 33°C). The difference between groups does not reach significance (WT, n = 8; $HetNa_v1.7^{I228M}$, n = 8; $HomNav1.7^{I228M}$, n = 8). (E) The thermal gradient test: the percentage of time spent at a range of temperature zones (6.5-46°C). No significant difference is seen between WT (n = 8), $HetNa_v1.7^{I228M}$ (n = 8), and $HomNa_v1.7^{I228M}$ (n = 8) groups. (F) The von Frey test for mechanical sensitivity ($Na_v1.7^{I228M}$ mutant mice by CRISPR gene editing). No significant difference is seen in withdrawal thresholds between WT (n = 7), $HetNa_v1.7^{I228M}$ (n = 5), and $HomNa_v1.7^{I228M}$ (n = 8). (G) The hot-plate test for thermal sensitivity at 50°C ($Na_v1.7^{I228M}$ mutant mice by CRISPR gene editing). No significant difference is seen between WT (n = 9), $HetNa_v1.7^{I228M}$ (n = 9), and $HomNa_v1.7^{I228M}$ (n = 5). (H) The thermal gradient test for thermal sensitivity ($Na_v1.7^{I228M}$ mutant mice by CRISPR gene editing). Freely moving animals placed on a gradient from 4 to 50°C did not show a difference in preferred temperature between WT (n = 7), $HetNa_v1.7^{I228M}$ (n = 10), and $HomNa_v1.7^{I228M}$ (n = 4).

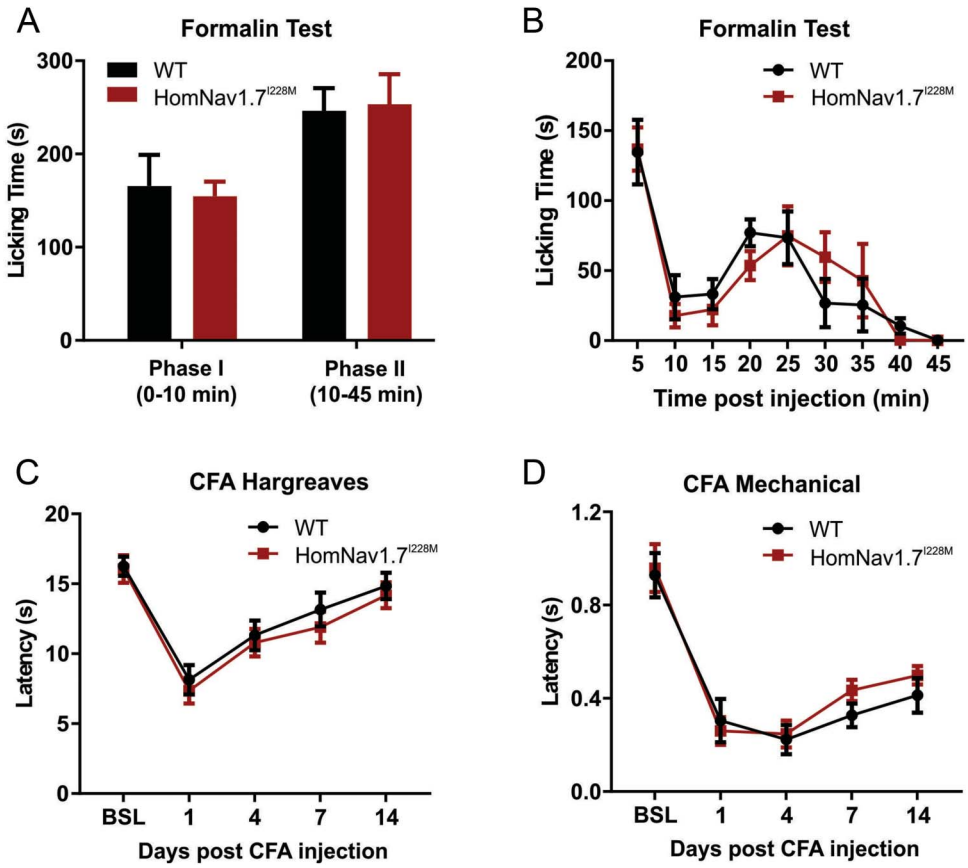

Figure 5. Behaviour responses of HomNa$_v$1.7^{I228M} mutant mice to formalin and CFA injections. (A and B) Formalin test. HomNa$_v$1.7^{I228M} mutant mice and their control littermates show similar licking durations in Phase I (WT, 165.6 ± 33.4 seconds, n = 5; HomNa$_v$1.7^{I228M}, 154.6 ± 15.8 seconds, n = 5) and Phase II (WT, 246.4 ± 24.2 seconds, n = 5; HomNa$_v$1.7^{I228M}, 253.4 ± 32.2 seconds, n = 5) of the formalin test. (C and D) Thermal and mechanical sensitivity measured by the Hargreaves test and von Frey test after intraplantar CFA injection. No significant difference is seen between WT (n = 11) and HomNav1.7^{I228M} (n = 12) groups. CFA, complete Freund's adjuvant; WT, wild type.

and mechanical stimuli assessed using the Hargreaves test and the von Frey test were also not significantly different between Na$_v$1.7^{I228M} mutant mice and wild-type controls (**Figs. 4B and C**). In the thermal preference test, Na$_v$1.7^{I228M} mice displayed normal warmth seeking (35 vs 25°C), cold avoidance (15 vs 25°C), and heat avoidance behaviours (38 vs 33°C) (**Fig. 4D**). The thermal gradient test (**Fig. 4E**) showed no difference between the genotypes. Behavioural examination in the CRISPR Na$_v$1.7 I228M knock-in line showed similar findings. No differences in the von Frey threshold (**Figs. 3F**), 50°C hot-plate response latency (**Fig. 4G**), or preferred temperature based on the thermal gradient test (**Fig. 4H**) were observed in these mice.

We also examined the impact of HomNav1.7^{I228M} on acute irritant-induced and inflammatory pain-related behavior induced by intraplantar injection of formalin or complete Freund's adjuvant (CFA), respectively. Behavioural responses (the duration of paw licking) in early and late phases of formalin test in HomNa$_v$1.7^{I228M} mutant mice produced by targeted homologous recombination were indistinguishable from those in control mice (**Figs. 5A and B**). Complete Freund's adjuvant injection induced long-lasting (up to 2 weeks) mechanical and thermal hypersensitivity in both HomNa$_v$1.7^{I228M} mutant mice and their wild-type control littermates. No statistical difference was observed between the groups (**Figs. 5C and D**).

3.4. Na$_v$1.7^{I228M} channels do not cause intraepidermal nerve fiber loss in mutant mice

As a variant associated with SFN, we tested whether Na$_v$1.7^{I228M} in mice had an impact on the integrity of distal nerve terminals. Using immunofluorescent staining, we evaluated the sensory innervation of the epidermis in skin biopsies taken from the same anatomical position in the ventral side of the glabrous foot pad from WT and Na$_v$1.7^{I228M} knock-in mice (targeted homologous recombination). As shown in **Figure 6A**, PGP9.5 staining of IENF is similar between WT and HomNa$_v$1.7^{I228M} mutant samples. Quantitative analysis did not reveal any statistical difference in IENF densities (WT, 19.6 ± 1.1/mm, n = 4; HomNa$_v$1.7^{I228M}, 17.0 ± 0.5/mm, n = 4; $P = 0.2$, Mann–Whitney test) (**Fig. 6B**). Semithin cross-sections of plastic-embedded sciatic nerve samples demonstrated that the gross morphology of myelinated axons and integrity of myelin sheaths seemed normal and groups of nonmyelinated axons (arrows) could be identified in both WT and HomNa$_v$1.7^{I228M} samples at the light microscopy level (×100) (**Fig. 6C**). Analysis of size distribution of myelinated axons in the tibial nerve showed that there was no significant difference between WT and HomNa$_v$1.7^{I228M} groups (**Fig. 6D**).

We next examined whether the presence of the gain-of-function I228M variant influenced the neurite integrity of red fluorescent protein-labelled DRG neurons in *in vitro* cultures from WT (**Fig. 7A**) and targeted recombination HomNa$_v$1.7^{I228M} mice (**Fig. 7B**). WT and HomNa$_v$1.7^{I228M} DRGs displayed similar neurite growth 7 days into culture (**Figs. 7C and D**). Quantification of the mean neurite

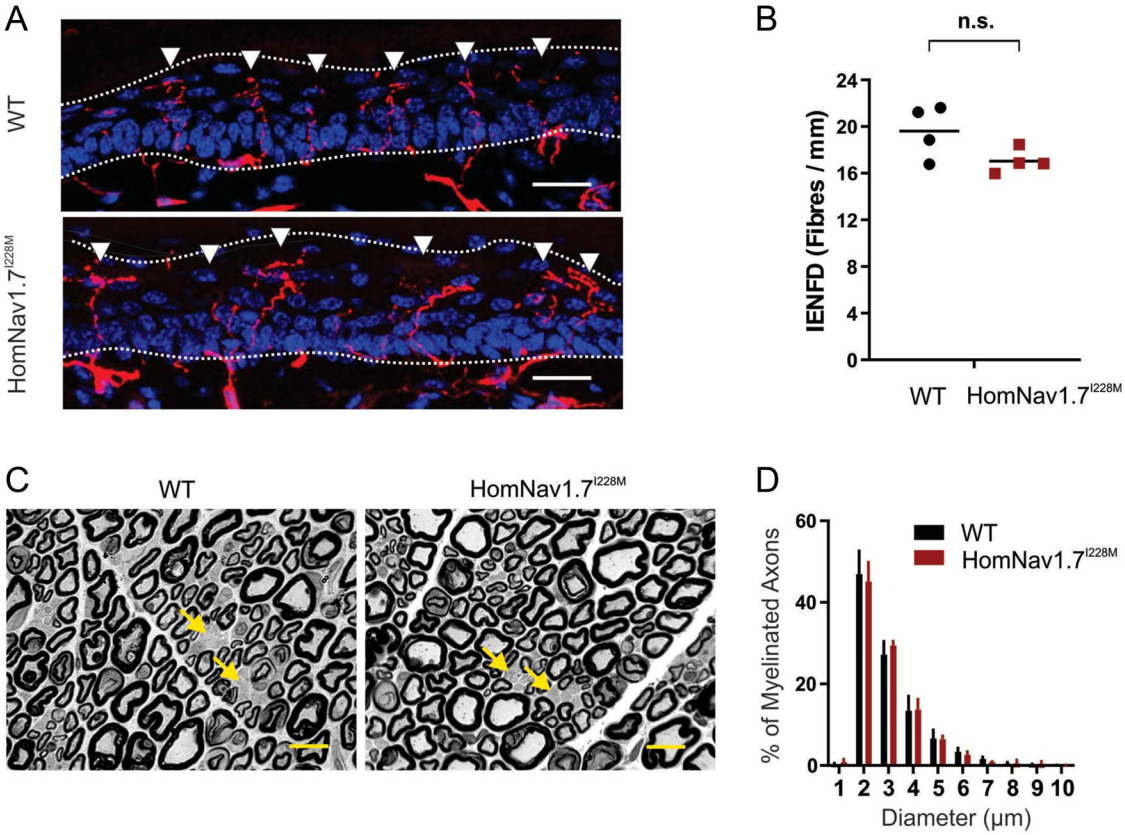

Figure 6. HomNa$_v$1.7^{I228M} mutant mice have normal intraepidermal nerve innervation and nerve fiber morphology. (A) Confocal images of intraepidermal nerve fibers (IENFs) in hind paw skin samples taken from WT and HomNa$_v$1.7^{I228M} mice. Intraepidermal nerve fibers labelled with the panaxonal marker PGP9.5 (red) extend from the subdermal plexus into the epidermis (nuclei labelled with DAPI, blue). The dashed line demarcates the division between the dermis and the epidermis layers. Scale bar = 20 μm. (B) Quantification of IENFs in hind paw skin samples taken from WT and HomNa$_v$1.7^{I228M} mice. The analysis shows no statistically significant difference in the IENF density (the unpaired student *t* test; WT, 19.6 ± 1.1/mm, n = 4; HomNa$_v$1.7^{I228M}, 17.0 ± 0.5/mm, n = 4). (C) Micrographs of semithin cross-sections of tibial branch of the sciatic nerve from WT and HomNa$_v$1.7^{I228M} mice. The morphology of the myelinated axons and unmyelinated axons (groups of unmyelinated axons in Remak bundles indicated by arrows) were all similar in WT and HomNa$_v$1.7^{I228M} mice. Images were taken by a light microscope at ×100. Scale bar = 10 μm. (D) Size distribution of myelinated axons in the tibial branch of sciatic nerves from WT (n = 3) and HomNav1.7^{I228M} (n = 3) mice. No significant differences exist between groups. WT, wild type.

length per cell calculated from large-field images showed that WT and HomNa$_v$1.7^{I228M} groups did not display any significant difference in the neurite lengths (WT 1.000 ± 0.1989, n = 19 cultures; HomNa$_v$1.7^{I228M} 1.039 ± 0.4898, n = 19 cultures; P = 0.8338, nested *t* test) (**Fig. 7E**).

In the CRISPR Na$_v$1.7^{I228M} KI mouse line, 24 hours after a monolayer culture, Tuj1-stained WT and HetNa$_v$1.7^{I228M} mutant DRG neurons appeared identical (**Figs. 7F and G**). Quantification of neurite length revealed no decrease in the length of HetNa$_v$1.7^{I228M} mutant neurons (**Fig. 7H**). Neurite length was also assessed by spot culture where neurons were plated in a dense spot, allowing neurites to grow radially outward for 6 days (**Fig. 7I**). Neurite length, quantified by Sholl analysis (the number of intersections of neurites with concentric rings drawn around the neuron), did not display a significant difference, supporting the conclusion that the Na$_v$1.7^{I228M} mutant did not impair neurite length in vitro (**Figs. 7J and K**).

4. Discussion

We established 2 independent Na$_v$1.7 I228M knock-in mouse lines, using both targeted homologous recombination and CRISPR editing. Using these mice, we provide the first detailed characterization of the excitability and axonal integrity of DRG neurons carrying the endogenous Na$_v$1.7 gain-of-function variant, I288M. We also tested here whether there were signs of the positive aspects of pain that have been reported in patients with SFN by inducing evoked responses to mechanical and thermal stimuli. We show that, although the presence of the I228M gain-of-function variant renders DRG neurons hyperexcitable, as expected, it does not alter thermal and mechanical sensitivity in these mice. In addition, at the age of the mice examined (up to 12 weeks when mice are considered adults (https://www.jax.org/news-and-insights/jax-blog/2017/november/when-are-mice-considered-old), the neurite/axonal integrity of cultured DRG neurons, the gross morphology of nerve fibers, and IENFD in skin biopsies were also not altered. Although the Na$_v$1.7 I228M knock-in in vivo mouse models provide a useful model of hyperexcitability in DRG neurons, we do not see evidence that such a functional change alone induces the genetically driven pain and neuropathy phenotype seen in patients with SFN carrying this mutation. This raises several interesting questions about the relationship between hyperexcitability, neuropathy, and pain and the utility of mouse models as surrogates of certain human disorders.

4.1. Mismatch between hyperexcitability of dorsal root ganglion neurons and the lack of behavioural phenotype

Previous work has suggested that hyperexcitability of small DRG neurons is a major driver of neuropathic pain.[1,6] However, because we found no indication of any alteration in pain-related behaviors in either mouse line, we suggest that in the case of the

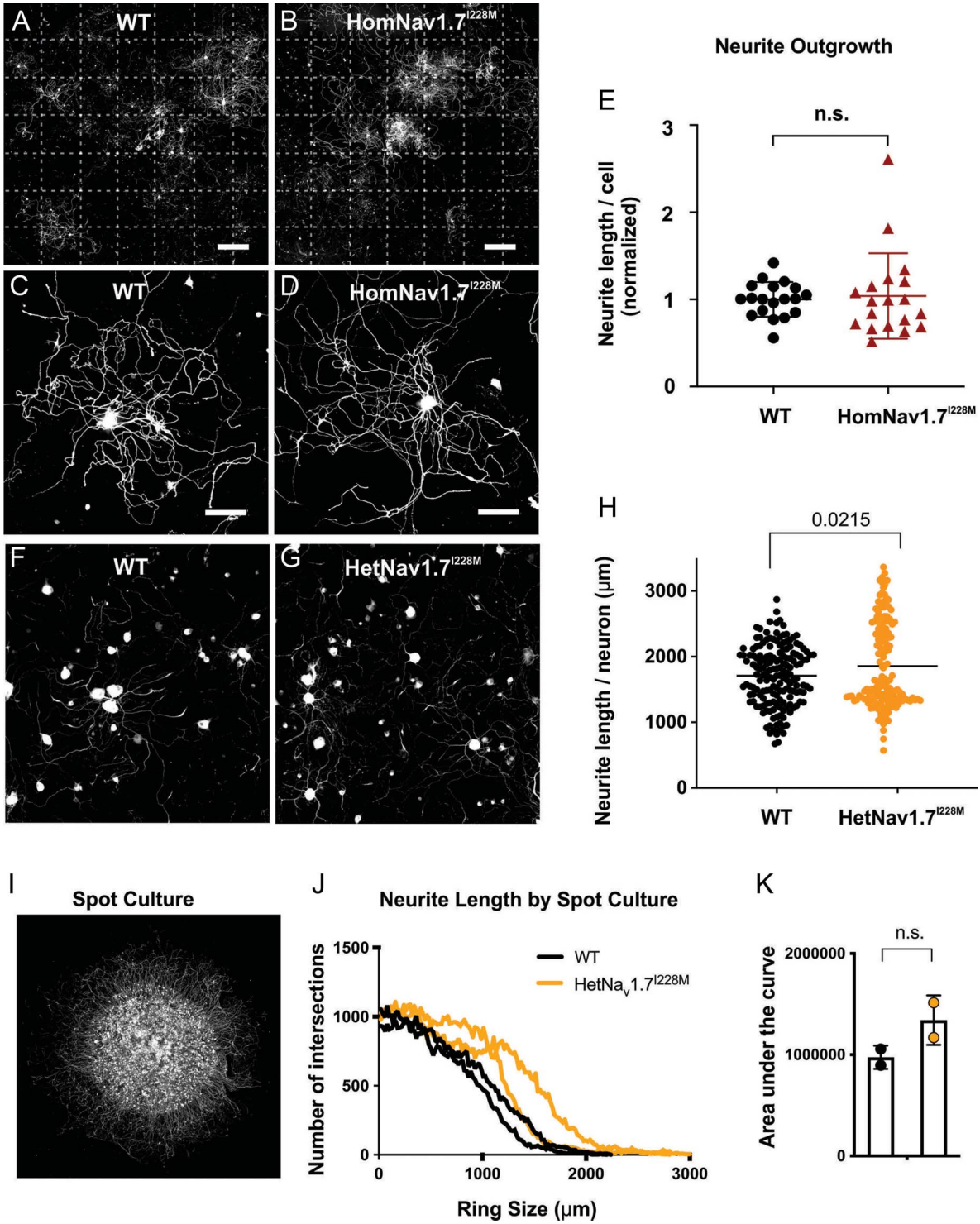

Figure 7. DRG neurons from HomNa$_v$1.7^{I228M} mutant mice display normal neurite length in vitro. (A–B) Representative large-field montage images of 7-day DRG cultures from (A) WT mice and (B) HomNa$_v$1.7^{I228M} mutant mice (6-8 weeks). Each large-field image consists of 7 × 7 field views. Dotted lines distinguish individual field-of-view. Scale bar, 1000 µm. (C–D) Representative images of individual (C) WT and (D) HomNa$_v$1.7^{I228M} DRG neurons with neurite growth. Scale bar, 50 µm. (E) Quantification of total length per cell of WT and HomNa$_v$1.7^{I228M} neurons. The average normalised neurite length per cell of WT (n = 19 culture dishes from 5 WT mice) and HomNa$_v$1.7^{I228M} (n = 19 culture dishes from 5 Na$_v$1.7 I228M mutant mice) is 1.000 ± 0.1989 and 1.039 ± 0.4898, respectively. There is no significant difference in neurite length (P = 0.8338, nested t test) between WT and HomNa$_v$1.7^{I228M} groups. (F–G) Representative images of (F) WT and (G) HetNa$_v$1.7^{I228M} DRG neurons (from HetNa$_v$1.7^{I228M} mutant mice by CRISPR gene editing) cultured in a monolayer, then fixed and stained with Tuj1 after 24 hours. (H) Neurites of cultured HetNa$_v$1.7^{I228M} neurons (n = 156 wells in a 96-well plate, from 4 HetNa$_v$1.7^{I228M} mutant mice by CRISPR gene editing) do not show evidence of degeneration and in fact display longer neurite lengths per neuron than WT (n = 167 wells in a 96-well plate, 4 mice) (P = 0.0215, two-tailed t test). (I) A example image of DRG neurons cultured in a spot culture, where neurons are plated in a dense spot, allowing neurites to grow radially outward. After 6 days of growth, neurons were fixed and stained with Tuj1. (J) Neurite length calculated by Sholl analysis, whereby the intersections of neurites with concentric rings drawn around the spot are quantified as a proxy for neurite length. Intersections at higher diameters indicate longer neurite lengths (WT, n = 2; HetNav1.7^{I228M} mutant by CRISPR gene editing, n = 2). (K) Area under the curve from (J). The area under the curve, representing the total neurite length per spot is not significantly different between WT and HetNa$_v$1.7^{I228M} (P = 0.195050, two-tailed t test). DRG, dorsal root ganglion; WT, wild type.

$Na_v1.7^{I228M}$ mutation, and potentially other gain-of-function $Na_v1.7$ mutations, the in vivo readout (behavior) might be modified or compensated for by additional factors that cannot be captured in the culture system. It is possible that in the case of this mutation the observed pain in patients is secondary to the neuropathy, which we do not see at the time-points measured in this study. This would be compatible with the decades it takes for pain to manifest in the patients. Further study into the relationship between the presence of a pain phenotype and the development of neuropathy in SFN in older mice will therefore be crucial. It is possible that in this mouse model and indeed in asymptomatic patients, developmental and compensatory changes within primary afferents or in spinal or supraspinal circuits mitigate the hyperexcitability effects of the mutation and in this way suppress pain hypersensitivity. In addition, the current standard methods used to detect pain-related behaviors in mice may also be a factor here.[2] Behavioural measures of pain in rodents are limited in scope, and standard stimulus-evoked assays may be too insensitive to detect alterations in pain. The reflex-based behavioural measures used in this study assess withdrawal latencies and responses to thermal and mechanical stimuli, but this may not capture the persistent spontaneous pain that characterizes patients with neuropathy.[3]

4.2. Lack of a neuropathy phenotype

Although the loss of IENF and presence of peripheral neuropathic pain as identified by quantitative sensory testing are used as the defining characteristics of SFN[4,11] and are present in patients with SFN carrying the $Na_v1.7$ I228M variant,[8,9] overall diagnostic criteria for SFN continue to be reevaluated.[3] The overexpression of I228M in vitro impairs the integrity of sensory axons, possibly through mechanisms involving an increase in local intracellular Ca^{2+} in neurites[13,14] and mitochondrial malfunction,[12] and transient overexpression of I228M in zebrafish embryos causes decreased nerve density and increased temperature-induced behaviour.[7] Through to 12 weeks of age in the 2 independently generated mouse lines, the endogenous I228M variant did not cause any observable morphological changes in distal axon terminals in the skin. It is possible that degeneration seen in *in vitro* studies was partially due to the increased load of mutant channels that is caused by the overexpression of the mutant channel. In addition, because degeneration in SFN is believed to occur in a dying-back fashion as a result of metabolic stress on long axons, the relative difference in axon length in mice and humans is a potential explanation for the lack of epidermal denervation in these mice. Although our current data does not preclude the possibility that a neuropathy phenotype may present beyond at a later stage, it did allow us to characterize the behavior of the mice at a time-point when their DRG neurons were hyperexcitable but their epidermal innervation remained intact. This provides insight into the question of whether the observed pain phenotype is due to hyperexcitability or to neuropathy, or a combination.

In 3 human patients with the $Na_v1.7^{I228M}$ mutation onset of neuropathic pain symptoms occurred at ages 32, 36, and 46 years.[8] Notably, 2 young adult sons of one patient harboured the I228M variant but did not have any SNF-like complaints at the time of study,[8] which might be viewed as a parallel to our findings. Our behavioural assessments were conducted in adult mice (up to 12 weeks), and it is possible that neuropathic pain-associated behaviour such as tactile allodynia might be observed at later time-points, secondary to the time-dependent development of neuropathy. This would leave unanswered, however, the discordance between DRG neuron hyperexcitability and the absence of demonstrable pain in the mouse lines we studied, and indeed presumably in asymptomatic patients. We suggest that although the $Na_v1.7$ variants and the associated sensory neuron hyperexcitability may be important risk factors, a secondary insult or aging may be required to cause intraepidermal nerve fiber degeneration, which may in turn trigger the neuropathic pain that is characteristic of SFN. I228M has been listed as a natural SNP in healthy control databases (103/60,146; gnomAD v2.1.1 Controls). A multihit model has been proposed to underlie the length dependence and age dependence of onset of peripheral neuropathies.[13] Other underlying factors, such as systemic diseases, modifier genes, or environmental factors, may be required, together with I228M, for the onset of clinical signs and symptoms of SFN, something not captured in the mouse models.

In conclusion, we have characterized 2 independent $Na_v1.7^{I228M}$ knock-in in vivo models generated with targeted homologous recombination and CRISPR gene editing, respectively. These parallel mouse lines with the endogenous $Na_v1.7$ I228M variant are the first mammalian models created for modelling $Na_v1.7$-related SFN to date. Although the mutant mice recapitulated the DRG neuronal hyperexcitability that is expected in patients with SFN with a gain-of-function mutation in Nav1.7, they do not recapitulate either the pain or neuropathy phenotypes seen in the patients. We believe that the hyperexcitability induced by this mutation in mice is not sufficient by itself to induce behavioural changes indicative of pain, at least in the absence of a neuropathy phenotype in mice. We would stress that a limitation of our study is that our electrophysiological studies were confined to the soma of DRG neurons, and recordings in vivo in both soma and nerve fibers will be needed to reach a more definitive answer on whether there is spontaneous firing of nociceptors. Nevertheless, our results suggest that DRG neuron hyperexcitability alone does not induce either SFN or a detectable pain phenotype in young adult mice. A parallel may exist in the clinical domain, where patients with $Na_v1.7$ mutations that presumably produce hyperexcitability in early development only develop pain in adulthood, potentially secondary to the development of neuropathy. The findings of this study underscore the complexity of the relationship between hyperexcitability, neuropathy, and pain in $Na_v1.7$ mutant generated SFN in an in vivo setting.

Conflict of interest statement

The authors have no conflicts of interest to declare.

Acknowledgements

The authors thank Dr Zhao Peng, Larry Macala, and Pamela Zwinger for their technical support. This work was supported by a grant from the Nancy Taylor Foundation, and Center Grant B9253-C from the US Department of Veterans Affairs Rehabilitation Research and Development Service (SDH and SGW). The Center for Neuroscience and Regeneration Research is a Collaboration of the Paralyzed Veterans of America with Yale University. This work was also supported by the NIH Award R35NS105076 (CJW) and a National Science Foundation fellowship (NKW).

Author contributions: L. Chen, N.K. Wimalasena, S.D. Dib-Hajj, C.J. Woolf, and S.G. Waxman designed research; L. Chen, N.K. Wimalasena, J. Shim, C. Han, S. Lee, R. Gonzalez-Cano, M. Estacion. C.G. Faber, and G. Lauria performed research and analyzed data; L. Chen, N.K. Wimalasena, S.G. Dib-Hajj, C.J. Woolf, and S.G. Waxman wrote the manuscript.

Article history:
Received 14 August 2020
Received in revised form 13 November 2020
Accepted 23 November 2020
Available online 11 December 2020

References

[1] Bennett DL, Clark AJ, Huang J, Waxman SG, Dib-Hajj SD. The role of voltage-gated sodium channels in pain signaling. Physiol Rev 2019;99:1079–151.
[2] Deuis JR, Dvorakova LS, Vetter I. Methods used to evaluate pain behaviors in rodents. Front Mol Neurosci 2017;10:284.
[3] Devigili G, Rinaldo S, Lombardi R, Cazzato D, Marchi M, Salvi E, Eleopra R, Lauria G. Diagnostic criteria for small fibre neuropathy in clinical practice and research. Brain 2019;142:3728–36.
[4] Devigili G, Tugnoli V, Penza P, Camozzi F, Lombardi R, Melli G, Broglio L, Granieri E, Lauria G. The diagnostic criteria for small fibre neuropathy: from symptoms to neuropathology. Brain 2008;131:1912–25.
[5] Dib-Hajj SD, Choi JS, Macala LJ, Tyrrell L, Black JA, Cummins TR, Waxman SG. Transfection of rat or mouse neurons by biolistics or electroporation. Nat Protoc 2009;4:1118–26.
[6] Dib-Hajj SD, Waxman SG. Sodium channels in human pain disorders: genetics and pharmacogenomics. Annu Rev Neurosci 2019;42:87–106.
[7] Eijkenboom I, Sopacua M, Otten ABC, Gerrits MM, Hoeijmakers JGJ, Waxman SG, Lombardi R, Lauria G, Merkies ISJ, Smeets HJM, Faber CG, Vanoevelen JM, Group PS. Expression of pathogenic SCN9A mutations in the zebrafish: a model to study small-fiber neuropathy. Exp Neurol 2019;311:257–64.
[8] Estacion M, Han C, Choi JS, Hoeijmakers JG, Lauria G, Drenth JP, Gerrits MM, Dib-Hajj SD, Faber CG, Merkies IS, Waxman SG. Intra- and interfamily phenotypic diversity in pain syndromes associated with a gain-of-function variant of NaV1.7. Mol Pain 2011;7:92.
[9] Faber CG, Hoeijmakers JG, Ahn HS, Cheng X, Han C, Choi JS, Estacion M, Lauria G, Vanhoutte EK, Gerrits MM, Dib-Hajj S, Drenth JP, Waxman SG, Merkies IS. Gain of function $Na_V1.7$ mutations in idiopathic small fiber neuropathy. Ann Neurol 2012a;71:26–39.
[10] Hoeijmakers JG, Faber CG, Lauria G, Merkies IS, Waxman SG. Small-fibre neuropathies-advances in diagnosis, pathophysiology and management. Nat Rev Neurol 2012b;8:369–79.
[11] Hoitsma E, Reulen JP, de Baets M, Drent M, Spaans F, Faber CG. Small fiber neuropathy: a common and important clinical disorder. J Neurol Sci 2004;227:119–30.
[12] Lee SI, Hoeijmakers JGJ, Faber CG, Merkies ISJ, Lauria G, Waxman SG. The small fiber neuropathy NaV1.7 I228M mutation: impaired neurite integrity via bioenergetic and mitotoxic mechanisms, and protection by dexpramipexole. J Neurophysiol 2020;123:645–57.
[13] Persson AK, Hoeijmakers JG, Estacion M, Black JA, Waxman SG. Sodium channels, mitochondria, and axonal degeneration in peripheral neuropathy. Trends Molecular Medicine 2016;22:377–90.
[14] Persson AK, Liu S, Faber CG, Merkies IS, Black JA, Waxman SG. Neuropathy-associated Na(V) 1.7 variant I228M impairs integrity of dorsal root ganglion neuron axons. Ann Neurol 2013;73:140–5.
[15] Themistocleous AC, Ramirez JD, Serra J, Bennett DL. The clinical approach to small fibre neuropathy and painful channelopathy. Pract Neurol 2014;14:368–79.